ARTICLE

doi:10.1038/nature22047

Cell diversity and network dynamics in photosensitive human brain organoids

Giorgia Quadrato[1,2], Tuan Nguyen[1,2], Evan Z. Macosko[2,3], John L. Sherwood[1,2], Sung Min Yang[1], Daniel R. Berger[4], Natalie Maria[1], Jorg Scholvin[5], Melissa Goldman[3], Justin P. Kinney[6], Edward S. Boyden[5], Jeff W. Lichtman[4], Ziv M. Williams[7], Steven A. McCarroll[2,3] & Paola Arlotta[1,2]

***In vitro* models of the developing brain such as three-dimensional brain organoids offer an unprecedented opportunity to study aspects of human brain development and disease. However, the cells generated within organoids and the extent to which they recapitulate the regional complexity, cellular diversity and circuit functionality of the brain remain undefined. Here we analyse gene expression in over 80,000 individual cells isolated from 31 human brain organoids. We find that organoids can generate a broad diversity of cells, which are related to endogenous classes, including cells from the cerebral cortex and the retina. Organoids could be developed over extended periods (more than 9 months), allowing for the establishment of relatively mature features, including the formation of dendritic spines and spontaneously active neuronal networks. Finally, neuronal activity within organoids could be controlled using light stimulation of photosensitive cells, which may offer a way to probe the functionality of human neuronal circuits using physiological sensory stimuli.**

In recent years, reductionist *in vitro* models of the developing human brain have emerged in the form of 3D human brain organoids and spheroids that are derived from pluripotent stem cells and are suitable for large-scale production and genetic engineering[1]. These systems offer an unprecedented opportunity to study both normal brain development and complex human diseases that affect multiple cell types, their interactions and the function of neuronal circuits.

Thus far, organoid models have been applied to study events of neural progenitor dysfunction that occur during early stages of brain development, including microcephaly-associated phenotypes[2] and progenitor abnormalities resulting from Zika virus infections[3–7]. Organoids generated from patients with severe idiopathic autism spectrum disorder have also been used to implicate progenitor overproliferation and generation of excessive GABAergic (γ-aminobutyric-acid-releasing) neurons in this complex disease[8]. However, difficulties remain that preclude the broader application of brain organoids to disease modelling[9].

Central issues include our incomplete understanding of the cellular composition of brain organoids, the potential of organoids to generate the regional and cellular diversity present in the brain and the reproducibility of the cell-type spectrum generated within individual organoids.

It is also essential to understand whether 3D brain organoids can continue to develop in culture past early developmental events, to allow not only the generation of endogenous cellular diversity, but also the maturation of neuronal networks, which will be needed to apply brain organoids to studies of late developmental events, such as complex cellular interactions and, most notably, higher-order brain functions that rely on functional neural networks.

Here we describe the prolonged development of human whole-brain organoids, and provide, to our knowledge, the largest-to-date molecular map of the diversity of cell types generated and its reproducibility across organoids. We show that organoids undergo substantial neuronal maturation, including generation of dendritic spines and the formation of spontaneously active neuronal networks. Finally, we demonstrate that neuronal activity within organoids is responsive to light-based stimulation of photosensitive cells, suggesting that organoid models may allow investigation of circuit functionality using physiological sensory mechanisms.

Protracted *in vitro* development of brain organoids

Human whole-brain organoids are largely self-patterning systems and therefore in principle have the potential to generate the vast cellular diversity of the endogenous tissue. However, this possibility remains largely untested. To address this point directly, we modified a previously described culturing protocol[2,10], to enable extended periods of growth and development. By seeding initial embryoid bodies with a reduced number of pluripotent stem cells (2,500 cells), optimizing neural induction and adding brain-derived neurotrophic factor (BDNF) to the final differentiation medium, we obtained long-term, progressive development for over nine months (Fig. 1a and Extended Data Fig. 1; see Methods). With this protocol, organoids do not become hypoxic and levels of programmed cell death remain relatively low up to nine months (Extended Data Fig. 1a). The yield of organoids from initial embryoid bodies was also improved, to more than 95% at one month with the human induced pluripotent stem cell line 11a (11a cells) and 70% for the human embryonic stem cell line HUES66.

To define the timeline of generation of broadly defined cell classes, we analysed a small set of informative single-gene markers by immunohistochemistry in organoids derived from the 11a cell line over one to nine months in culture (Extended Data Fig. 1b, c and Supplementary Discussion). At one month, organoids showed early brain regionalization, expressing markers for germinal zones of the forebrain (PAX6 and NKX2.1), midbrain (OTX2), hindbrain (GBX2) and retina (VSX2, OTX2) (Extended Data Fig. 1c, d). Resembling the endogenous sequence, neural progenitors emerged first, followed by

[1]Department of Stem Cell and Regenerative Biology, Harvard University, Cambridge, Massachusetts 02138, USA. [2]Stanley Center for Psychiatric Research, Broad Institute of Harvard and MIT, Cambridge, Massachusetts 02142, USA. [3]Department of Genetics, Harvard Medical School, Boston, Massachusetts 02115, USA. [4]Department of Cellular and Molecular Biology and Center for Brain Science, Harvard University, Cambridge, Massachusetts 02138, USA. [5]Departments of Biological Engineering and Brain and Cognitive Sciences, MIT Media Lab and McGovern Institute, MIT, Cambridge, Massachusetts 02139, USA. [6]LeafLabs, LLC, Cambridge, Massachusetts 02139, USA. [7]Department of Neurosurgery, Massachusetts General Hospital, Harvard Medical School, Boston, Massachusetts 02114, USA.

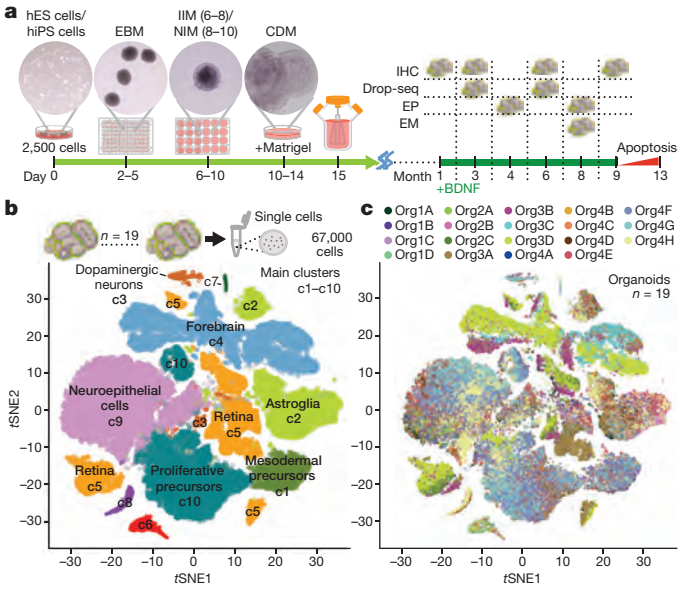

Figure 1 | Large-scale, single-cell sequencing demonstrates development of a broad spectrum of cell types in human brain organoids. a, Left, schematic of long-term culture of brain organoids. Dissociated human induced pluripotent stem cells are seeded at day 0 into round-bottom plates to allow embryoid body formation (day 2–5). After a two-step neural induction (day 6–10), embryoid bodies are embedded in Matrigel (day 10) and transferred to spinning bioreactors (day 15) for long-term culture. BDNF is added starting at one month. CDM, cerebral differentiation medium; EBM, embryoid body medium; IIM, intermediate induction medium; NIM, neural induction medium. Right, immunohistochemistry (IHC), single-cell RNA sequencing (Drop-seq), electrophysiology (EP) and electron microscopy (EM) were performed at different time points. **b**, *t*-distributed stochastic neighbour embedding (*t*SNE) plot of single-cell mRNA sequencing data from six-month-old organoids. A total of 66,889 cells were clustered into 10 distinct groups. **c**, Same as in **b**, with cells colour-coded by organoid (Org) of origin.

glutamatergic, GABAergic and dopaminergic neuronal identities and GFAP$^+$ astroglia. The data indicate that whole brain organoids can develop for long periods of time and have the potential to generate cell types from distinct germinal zones of the brain and retina.

Large single-cell map of cell diversity in organoids

Individual gene markers cannot resolve the cellular diversity of the human brain, in which closely related cell classes can only be identified using combinatorial gene signatures. Single-cell RNA sequencing allows systematic analysis of many genes, but the cellular diversity of the human brain requires that very large numbers of cells be profiled. To address this issue directly, we used droplet-based single-cell mRNA sequencing (Drop-seq)[11] to molecularly profile 82,291 single cells isolated from 31 organoids that were derived from a healthy-control induced pluripotent stem cell line (11a cells) at three and six months *in vitro*.

Starting with a relatively advanced stage of development, six months, we analysed an average of 3,520 cells per organoid from each of 19 organoids grown in four separate bioreactors (range of 1,656–11,061 cells per organoid). Principal component analysis of read counts was performed with dimensionality reduction using *t*-distributed stochastic neighbour embedding[12–14] (see Methods). Clustering all cells from the six month organoids produced ten main transcriptionally distinct populations (Fig. 1b). We systematically compared the differentially expressed gene signatures for each cluster to gene signatures extracted from existing RNA-sequencing (RNA-seq) datasets of endogenous cell types[11,15–27] (Extended Data Fig. 2). We were able to define the identities of the seven largest clusters (c1, c2, c3, c4, c5, c9 and c10) (Fig. 1b).

Six of the seven clusters belonged to the neurectodermal lineage; however, one cluster (c1; 3,027 cells) expressed mesodermal markers, including myogenin and myosin genes (*MYH3*, *MYH8*, *MYL1* and *MYLPF*), indicating that, despite early patterning to a neurectodermal fate, organoids can still produce a minority of cells of another embryonic origin.

Cluster c2 (8,409 cells) was primarily composed of cells expressing genes of endogenous adult human astrocytes[27], including canonical astrocyte markers *AQP4* and *GFAP*. Cluster c9 (17,103 cells) contained progenitors of neuroepithelial origin, including cells with an oligodendrocyte-precursor-like identity[20,26]. Cluster c10 (13,428 cells) was mainly composed of cells with signatures of highly proliferative progenitors (for example, *TOP2A* and *MKI67*). Cluster c3 (971 cells) was enriched for cells expressing neuronal genes, including dopaminergic markers (for example, *TH* and *EBF1*). Perhaps the most notable clusters were c4 and c5 (12,378 and 9,919 cells, respectively) (Fig. 2a–d). Cluster c4 had a clear neuronal signature and was enriched for markers of neurons and progenitors of the cerebral cortex. Cluster c5 (9,919 cells) showed a strong representation of genes of the neural retina, such as the photoreceptor markers *CRX* and *RCVRN*[28,29]. Comparison with several gene expression datasets of the mouse and human retina[11,23,24] confirmed that this cluster was composed predominantly of retinal cells.

To quantify variability among organoids and possible bioreactor-based batch effects, we determined the frequency with which cells from each of the ten clusters were generated in individual organoids and across bioreactors (Fig. 1c, Extended Data Fig. 3 and Supplementary Discussion). We found that most clusters were consistently represented (c1, c2, c5, c9, c10, which were each found in more than 89% of organoids), although clusters c3 and c4 were present in only a subset of organoids (53% and 32%, respectively). Notably, organoids grown in the same bioreactor were more similar to one another in their ability to make cells of each cluster (for example, 100% of organoids from bioreactor 3 contained the forebrain cluster), suggesting that bioreactor-related growth environment is a key factor in controlling cell class identity (Extended Data Fig. 3 and Supplementary Discussion).

Endogenous and organoid cellular diversity correlate

In order to understand to what degree endogenous cellular diversity is generated within organoids, we more closely dissected the forebrain and retinal clusters (c4 and c5) by a second iteration of clustering. Within cluster c4, we identified 30 transcriptionally distinct subclusters (Fig. 2a and data not shown); we were able to assign 17 of these to 5 broad cell-type identities (Fig. 2a). Subclusters 7–8 and 9–15 included putative corticofugal and callosal projection neurons, respectively. Subclusters 16–23 were enriched for human radial glia markers[22], whereas subcluster 4 was distinguished by the expression of canonical genes of intermediate progenitors, including *EOMES* and *ELAVL4*. Finally, subcluster 1 displayed molecular signatures of interneurons, including *DLX5*, *DLX2*, *SCGN* and *GAD1*.

We confirmed this similarity by correlating subcluster gene signatures with a previously published single-cell RNA-seq dataset of the human fetal cortex[22] (see Methods). Despite the differences in the profiling methods used (Drop-seq compared to Fluidigm C1), we detected appropriate, preferential correlation between corresponding cell types for radial glia, interneurons, projection neurons and induced pluripotent stem cells (Extended Data Fig. 4a).

Next, we examined the subclusters of the retinal cluster (c5). Using class-specific retinal markers identified in a previous Drop-seq analysis of 44,408 single cells from the mouse retina[11], we found that cluster c5 contained almost all of the cell classes found in the mouse retina. Specifically, we identified populations that expressed marker genes for Müller glial cells (for example, *DKK3*, *SOX9*), pigmented epithelial cells (for example, *MLANA*, *MITF*), photoreceptors (for example, *CRX*, *RCVRN*, *NRL*), retinal ganglion cells (for example, *NEFL*, *NEFM*), bipolar cells (for example, *LHX4*, *PCP2*) and amacrine cells (for example, *TFAP2B*,

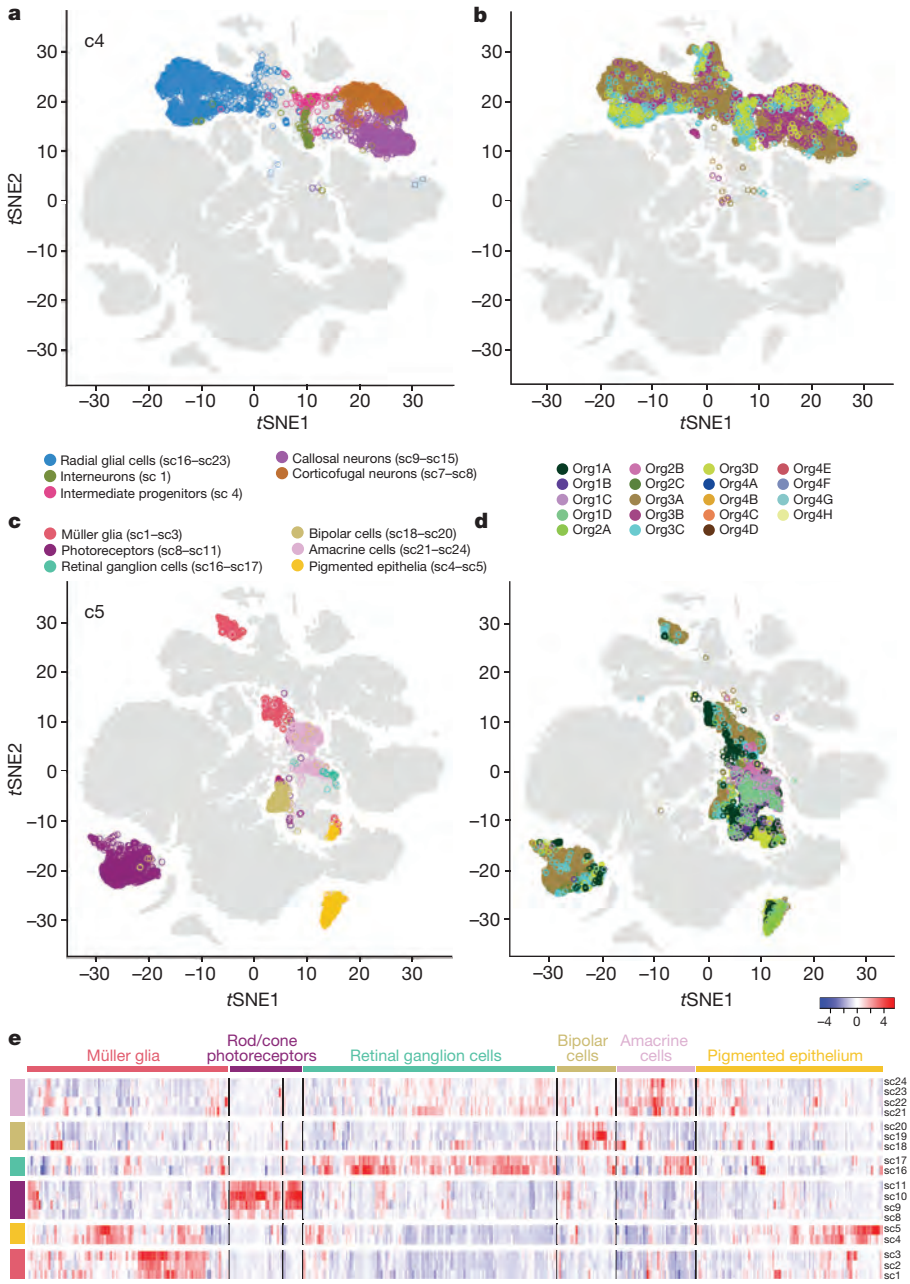

Figure 2 | Human brain organoids contain subclasses of forebrain and retinal cells. a, Subclustering of the forebrain cluster (c4): five major cell subtypes were identified as radial glia (7 subclusters), interneurons (1 subcluster), intermediate progenitors (1 subcluster), corticofugal neurons (2 subclusters) and callosal neurons (8 subclusters). sc, subcluster. **b**, All cells in c4, colour-coded by organoid of origin. **c**, Subclustering of the retinal cluster (c5): six major cell subtypes were identified as Müller glia (3 subclusters), photoreceptors (4 subclusters), retinal ganglion cells (2 subclusters), bipolar cells (3 subclusters), amacrine cells (4 subclusters) and pigmented epithelium (2 subclusters). **d**, All cells in c5, colour-coded by organoid of origin. **e**, Expression of genes identified as retinal cell subtype markers across the retinal subclusters (see Extended Data Fig. 2c for sources).

SLC32A1) (Fig. 2c, e). To validate these identities, we correlated subcluster gene signatures to the mouse retina Drop-seq dataset[11] (see Methods). Each of the organoid retinal populations showed strong correlation to the expected mouse retinal-cell class (Extended Data Fig. 5b).

Taken together, these analyses indicate that distinct cell types generated in organoids transcriptionally resemble the appropriate endogenous counterparts from the human fetal cortex and mouse retina.

To assess variability in cell-type production, we examined organoids from bioreactors in which all organoids generated forebrain (bioreactor 3) or retina (bioreactors 1, 2 and 3) (Fig. 2b, d, Extended Data Fig. 4a–c and Supplementary Discussion). For the forebrain, callosal projection neurons and radial glia progenitors were present in all organoids sampled, whereas cortical interneurons, corticofugal projection neurons and intermediate progenitors were present in 50% of the organoids. For the retina, photoreceptors and pigmented epithelial cells developed in the majority of organoids (73% and 91%, respectively), whereas development of retinal ganglion cells, bipolar cells and amacrine cells (each around 55%) and Müller glia (36%) occurred more sporadically (Extended Data Fig. 4b, d). This analysis probably overestimates the true variability, given the relatively small number of cells in each subcluster that were sampled from each organoid, and differences between cell types in robustness to dissociation and collection; indeed, immunohistochemistry for known markers indicates a higher frequency of co-development of the same putative populations (Extended Data Fig. 4a, c and Supplementary Discussion).

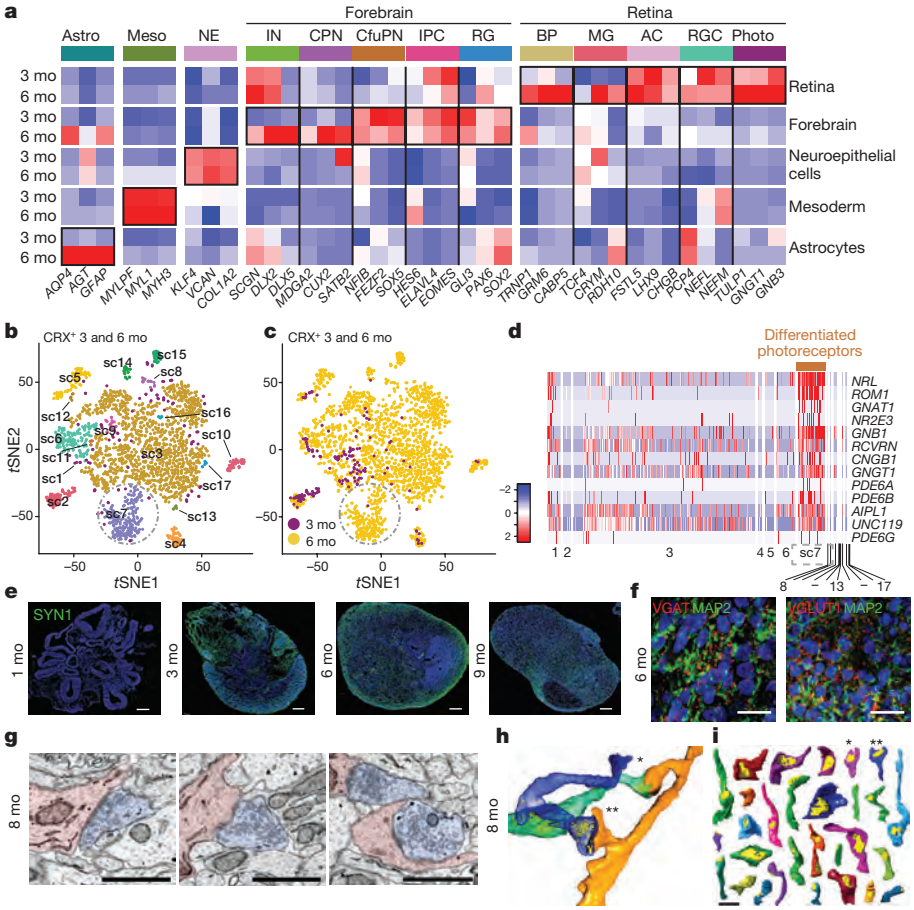

Figure 3 | Extended culture allows development of mature cell types including differentiated photoreceptors. **a**, Average expression of selected marker genes in organoids, by cell type and organoid age (three months (mo) compared to six months). AC, amacrine cells; astro, astrocytes; BP, bipolar cells; CfuPN, corticofugal projection neurons; CPN, callosal projection neurons; IN, interneurons; IPC, intermediate progenitor cells; meso, mesodermal cells; MG, Müller glia; NE, neuroepithelial cells; photo: photoreceptors; RG, radial glial cells; RGC, retinal ganglion cells. **b**, Reclustering of CRX$^+$ cells in the combined three-month and six-month datasets identifies 17 clusters. **c**, Among CRX$^+$ cells, subcluster 7 is present only at six months. **d**, Genes related to rod phototransduction (brown bar) are highly differentially expressed in the photoreceptor cluster (subcluster 7). **e**–**i**, Synapse and dendritic spine development in organoids. **e**, Expression of the synaptic marker SYN1 is absent at one month and appears with organoid maturation by three months. **f**, Immunohistochemical detection of the synaptic proteins VGAT (left) and VGLUT1 (right) in a six-month-old organoid. **g**, Example electron microscopy images of synaptic structures in the reconstructed volume. **h**, Example dendrite with two spines (orange) making synapses with two axons (blue and green). Synaptic vesicles, yellow. **i**, Synaptic contact sites (yellow) on the 29 innervated spines identified in the volume. The spines reconstructed in **h** are indicated in **i**, by one and two asterisks, respectively. Scale bars, 250 μm (**e**), 20 μm (**f**) and 1 μm (**g**, **i**).

Enhanced development and maturation of organoids

To evaluate whether additional cell types progressively emerged and greater maturation occurred over time in culture, we performed Drop-seq analysis on an additional 15,402 cells from three-month-old organoids. We found that although some cell types were present at both three and six months, some appeared only at six months. Of note, at three months the forebrain cluster did not contain the population of putative callosal projection neurons, which *in vivo* are born in large numbers during late corticogenesis. Similarly, Müller glial and bipolar cells, which are normally generated at late stages of retinal development, were absent from the three month dataset (Fig. 3a).

We next identified populations that were present at both three and six months and compared their molecular signatures between ages. First, we analysed cells in the retinal cluster that expressed the transcription factor *CRX*, which marks both developing and mature photoreceptors. Clustering all *CRX*-positive cells across both three and six months organoids identified a subcluster (subcluster 7, 871 cells), which contained mature photoreceptors (Fig. 3b–d and Methods). Notably, all but one of the cells in this cluster came from the six months dataset (Fig. 3c).

Cells that had a putative corticofugal projection neuron identity were present in both three- and six-month-old organoids and showed similar progressive maturation: functional clustering of gene sets (using DAVID 6.7 (ref. 30)) revealed a clear enrichment for genes involved in neuronal maturation at six months, but not at three months (data not shown). Finally, cells expressing astroglial markers at three months lacked markers of mature astrocytes (that is, *GFAP*, *AQP4* and *AGT*), which were present only at six months (Fig. 3a).

We then investigated whether the maturation of cells, which were detected by molecular profiling, was also reflected in structural traits of more mature neurons, including formation of synapses and the presence of dendritic spines.

The presynaptic marker synapsin 1 (*SYN1*) was absent at one month, but began to be expressed at three months, persisting for at least nine months (Fig. 3e). Detection of VGAT$^+$ and VGLUT1$^+$ puncta suggested that both glutamatergic and GABAergic synapses were present (Fig. 3f). Electron microscopy imaging of an organoid at eight months (Extended Data Fig. 6), confirmed the presence of many structurally defined synapses (Fig. 3g).

Next, we used serial electron microscopy to analyse neuronal morphology, and in particular dendritic spines, which are notoriously difficult to generate *in vitro* because neurons that have been derived from pluripotent stem cells typically retain an embryonic identity. We reconstructed a region of approximately $16 \times 16 \times 5.4\,\mu m$ of an eight-month-old organoid and identified a total of 129 synapses (0.088 synapses per μm^3, which is approximately in the range of human fetal cortex[31]; see Supplementary Discussion) (Fig. 3g and Supplementary Videos 1, 2). We analysed 100 of these synapses; with two exceptions (two objects that were both receiving and making synapses), processes were either exclusively presynaptic (57 objects, axons) or exclusively postsynaptic (54 objects, dendrites), often making more than one synapse in the volume. The labelled dendrites had a total of 37 spines, which were variable in shape, but were often innervated by a synapse; 30 of these synapses were made on spines (Fig. 3h, i and Supplementary Video 3).

These data indicate that long-term culture of human brain organoids allows continuing development to ultimately produce great cellular diversity and unprecedented neuronal maturation.

Active neuronal networks in photosensitive organoids

Given the enhanced maturity of the neurons that were generated, we investigated whether spontaneously active neuronal networks were present. We performed extracellular recordings with high-density silicon microelectrodes[32] (Fig. 4a and Extended Data Fig. 7a), and

were able to isolate spikes in 6 out of 7 eight-month-old organoids (11 recording sites, 32 units in total), with a median mean-firing rate of 0.66 Hz (1st–3rd quantile (Q1–3) = 0.20–2.08 Hz). Spike rate was suppressed by bath application of tetrodotoxin (2 μM), a voltage-gated sodium-channel antagonist ($n = 4$ organoids; data not shown); together with the correspondence of the unit waveforms to standard structure and the presence of typical refractory periods (Fig. 4b and Extended Data Fig. 7b), this indicates that the isolated spikes are action potentials. By contrast, no spontaneously firing neurons were detected in four-month-old organoids ($n = 4$ organoids; Fig. 4c), in line with the progressive maturation seen in our single-cell transcriptome data.

To determine if active neurons were functionally connected, we analysed the spike train cross-correlograms and detected positive peaks with a short lag time, indicative of excitatory monosynaptic connections[33,34] (Fig. 4d). Bath application of 20 μM NBQX (2,3-dioxo-6-nitro-1,2,3,4-tetrahydrobenzo[*f*]quinoxaline-7-sulfonamide)[35] significantly reduced the firing rate by 81% (Fig. 4e), suggesting that the majority of recorded spikes were being driven by non-NMDA receptor-mediated excitatory synaptic transmission.

We next assessed active neuronal networks by examining population firing characteristics. In all spontaneously active organoids ($n = 6$), for the majority of isolated units, the statistical structure of the time series indicated the presence of network activity (Extended Data Fig. 7d). Three of these organoids displayed obvious burst firing patterns (Fig. 4f, bottom), whereas the remaining three organoids showed relatively stable firing patterns (Fig. 4f, top). In organoids with a burst pattern, we observed sets of neurons that displayed periods of coordinated activity (that is, population bursts; three recording sites from two organoids). Notably, within these periods the order of neuronal recruitment and firing showed a clear and reproducible temporal structure (Fig. 4g), that was reflected by asymmetry in the cross-correlograms (Extended Data Fig. 7g). These results suggest that brain organoids establish neuronal networks that can support self-organized patterns of activity.

Our single-cell RNA-seq analysis indicates that long-term cultures of human brain organoids support the differentiation of photoreceptor-like cells equipped with key proteins for light responsiveness. This is in agreement with the finding that retinal organoids contain photosensitive cells[36]. We therefore tested whether light-based physiological sensory stimuli could modulate neuronal activity. We investigated the effect of 530 nm light on the firing rate of 25 cells recorded from 10 organoids (7–9 months), and identified a subpopulation of neurons that displayed attenuated firing rates after light exposure (4 out of the 10 organoids that were tested had light-responsive units, Fig. 4h and Extended Data Fig. 7h, i). In agreement, the activity-dependent gene FOS was upregulated in eight-month-old organoids after light exposure (Fig. 4i). The data indicate that brain organoids establish spontaneously active neuronal networks and generate functional photosensitive cells, which may in the future permit modulation of network activity using physiological sensory mechanisms.

Discussion

Human brain organoids have enormous potential to serve as *in vitro* models of the human brain. Fulfilment of this promise, however, requires a deeper knowledge of their cellular composition, and a better understanding of the extent and reproducibility with which they generate the cellular diversity of the brain, produce mature neuronal traits and develop functional neuronal networks. We used a high-throughput single-cell transcriptional profiling method to establish that human whole-brain organoids can achieve extensive development and maturation and generate an unprecedented diversity of cell types. In agreement with prior work that had examined a smaller number of cells from early-stage organoids[17], the cells generated are closely related to their endogenous counterparts of the brain and retina.

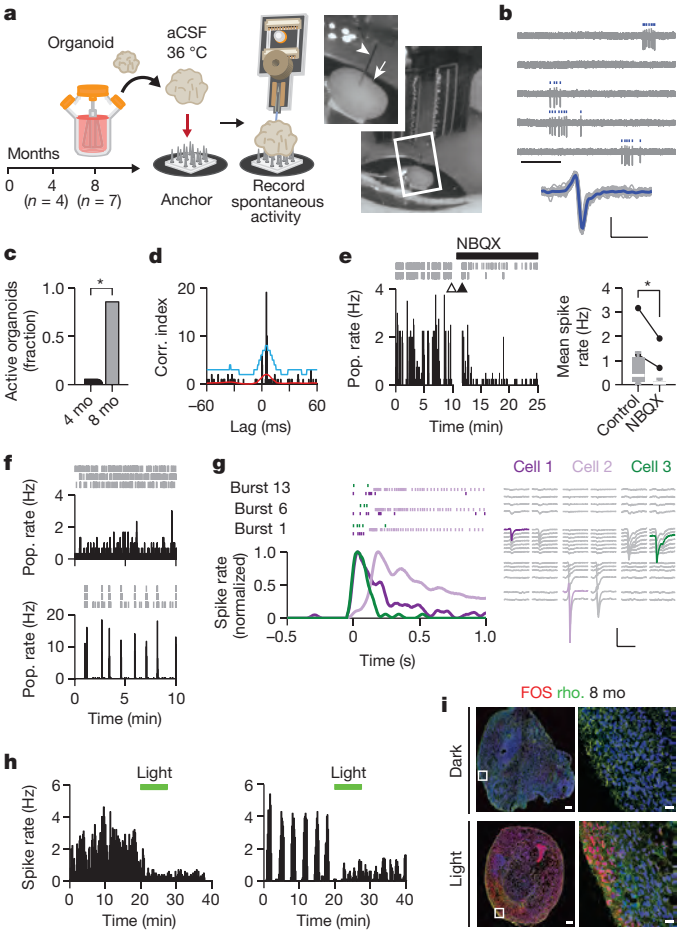

Figure 4 | Brain organoids develop spontaneous networks and photosensitive neurons that can be modulated by sensory stimulation with light. a, Schematic (left) and photograph (right) of extracellular recordings from intact organoids. Arrowhead, probe shank; arrow, organoid. aCSF, artificial cerebrospinal fluid. **b**, Human brain organoids display spontaneous activity. Top, example raw traces and spike raster plots from a single unit. Scale bar, 0.5 s. Bottom, individual (grey) and average (blue) spike waveforms. Scale bars, 0.5 ms (horizontal), 50 μV (vertical). **c**, Organoids display spontaneous activity at eight months (6 out of 7) but not four months (0 out of 4; Fisher's exact test, $*P = 0.015$). **d**, Example spike-train cross-correlogram. The positive peak with a short time lag indicates mono-synaptic connections. Red line, estimated mean spike rate; blue line, statistical threshold for identification of connected pairs (see Methods). Corr., correlation. **e**, NBQX attenuates activity. Left, example raster plots and population-averaged spiking rate (pop. rate). 2 s bins; arrowheads indicate break to apply NBQX. Right, summary plot ($n = 12$; control, median = 0.380 Hz, Q1–3 = 0.115–1.145; NBQX, median = 0.073 Hz, Q1–3 = 0.007–0.163; exact sign test, $*P < 0.0005$). Box plots show the median (line) and Q1–Q3 (box); inter-quartile range, IQR = Q3−Q1; whiskers extend to the most extreme data points between Q1 − (1.5 × IQR) and Q3 + (1.5 × IQR). Paired measurements, where either of the two points fall outside the whiskers, are illustrated as connected dots. **f**, Example population rate histograms (1 s bins), for organoids displaying bursts of activity (bottom) and without obvious activity bursts (top). Inset, raster plots of isolated units. **g**, Neuronal activity during population bursts shows a temporal structure. Left, neuron mean firing rate aligned to burst onset and raster plots for three neurons (colour-coded) in three example bursts. Right, mean spike waveforms recorded by probes (colour, peak response; vertical order reflects probe geometry). Scale bars, 2 ms (horizontal), 50 μV (vertical). **h**, Example rate histograms (10 s bins) for two cells showing light-attenuated activity (see Extended Data Fig. 7 h–i). **i**, Light stimulation increases FOS expression (red); rod-like cells are indicated by rhodopsin staining (rho.; green). Scale bars, 250 μm and 20 μm (inset).

In addition to mapping cellular diversity in organoids, we provide a first measure of the organoid-to-organoid variability in the generation of each cell type, and identify types that are reproducibly generated and others that appear more sporadically. Notably, this variability relates at least partly to bioreactor-based batch effects, suggesting a need for strategies to better control growth environment or to identify 'successful' bioreactors a priori.

We find that upon maturation organoids acquire structural traits of mature neurons, including dendritic spine-like structures, which have been difficult to generate by *in vitro* directed differentiation. This offers the opportunity to study a new set of developmental processes, such as human synaptic pruning and active spine refinement, which could not previously be modelled *in vitro*.

By eight months, whole-brain organoids also generate spontaneously active neurons and neuronal networks, as well as photosensitive cells that can respond to non-invasive, light-based sensory stimulation. While we could not determine whether light directly alters the activity of photosensitive cells or modulates downstream neuronal networks, the work suggests that this model may make it possible to study the response of neuronal networks to physiological sensory stimuli, in parallel with engineered optogenetic systems. In future work, it will be important to identify the neuron types participating in these networks, ideally through strategies that link whole-cell patch-clamp recordings to single-cell transcriptomes.

The diversity and maturation of cell types generated, the robustness of the neuronal networks, the presence of structural traits of mature neurons and the possibility of using sensory experience to modulate neuronal activity collectively suggest that, beyond modelling early events of progenitor biology, these 3D brain organoids have the potential to model higher-order functions of the human brain, such as cellular interactions and neural circuit dysfunctions related to neurodevelopmental and neuropsychiatric pathologies.

Online Content Methods, along with any additional Extended Data display items and Source Data, are available in the online version of the paper; references unique to these sections appear only in the online paper.

Received 17 August 2016; accepted 7 March 2017.
Published online 26 April 2017.

1. Kelava, I. & Lancaster, M. A. Stem cell models of human brain development. *Cell Stem Cell* **18,** 736–748 (2016).
2. Lancaster, M. A. *et al.* Cerebral organoids model human brain development and microcephaly. *Nature* **501,** 373–379 (2013).
3. Cugola, F. R. *et al.* The Brazilian Zika virus strain causes birth defects in experimental models. *Nature* **534,** 267–271 (2016).
4. Dang, J. *et al.* Zika virus depletes neural progenitors in human cerebral organoids through activation of the innate immune receptor TLR3. *Cell Stem Cell* **19,** 258–265 (2016).
5. Garcez, P. P. *et al.* Zika virus impairs growth in human neurospheres and brain organoids. *Science* **352,** 816–818 (2016).
6. Nowakowski, T. J. *et al.* Expression analysis highlights AXL as a candidate Zika virus entry receptor in neural stem cells. *Cell Stem Cell* **18,** 591–596 (2016).
7. Qian, X. *et al.* Brain-Region-specific organoids using mini-bioreactors for modeling ZIKV exposure. *Cell* **165,** 1238–1254 (2016).
8. Mariani, J. *et al.* FOXG1-dependent dysregulation of GABA/glutamate neuron differentiation in autism spectrum disorders. *Cell* **162,** 375–390 (2015).
9. Quadrato, G., Brown, J. & Arlotta, P. The promises and challenges of human brain organoids as models of neuropsychiatric disease. *Nat. Med.* **22,** 1220–1228 (2016).
10. Lancaster, M. A. & Knoblich, J. A. Generation of cerebral organoids from human pluripotent stem cells. *Nat. Protocols* **9,** 2329–2340 (2014).
11. Macosko, E. Z. *et al.* Highly parallel genome-wide expression profiling of individual cells using nanoliter droplets. *Cell* **161,** 1202–1214 (2015).
12. Satija, R., Farrell, J. A., Gennert, D., Schier, A. F. & Regev, A. Spatial reconstruction of single-cell gene expression data. *Nat. Biotechnol.* **33,** 495–502 (2015).
13. Amir, A. D. *et al.* viSNE enables visualization of high dimensional single-cell data and reveals phenotypic heterogeneity of leukemia. *Nat. Biotechnol.* **31,** 545–552 (2013).
14. van der Maaten, L. & Hinton, G. Visualizing data using t-SNE. *J. Mach. Learn. Res.* **9,** 2579–2605 (2008).
15. Arlotta, P. *et al.* Neuronal subtype-specific genes that control corticospinal motor neuron development *in vivo*. *Neuron* **45,** 207–221 (2005).
16. Cahoy, J. D. *et al.* A transcriptome database for astrocytes, neurons, and oligodendrocytes: a new resource for understanding brain development and function. *J. Neurosci.* **28,** 264–278 (2008).
17. Camp, J. G. *et al.* Human cerebral organoids recapitulate gene expression programs of fetal neocortex development. *Proc. Natl Acad. Sci. USA* **112,** 15672–15677 (2015).
18. Darmanis, S. *et al.* A survey of human brain transcriptome diversity at the single cell level. *Proc. Natl Acad. Sci. USA* **112,** 7285–7290 (2015).
19. Lake, B. B. *et al.* Neuronal subtypes and diversity revealed by single-nucleus RNA sequencing of the human brain. *Science* **352,** 1586–1590 (2016).
20. Marques, S. *et al.* Oligodendrocyte heterogeneity in the mouse juvenile and adult central nervous system. *Science* **352,** 1326–1329 (2016).
21. Molyneaux, B. J. *et al.* Novel subtype-specific genes identify distinct subpopulations of callosal projection neurons. *J. Neurosci.* **29,** 12343–12354 (2009).
22. Pollen, A. A. *et al.* Molecular identity of human outer radial glia during cortical development. *Cell* **163,** 55–67 (2015).
23. Siegert, S. *et al.* Transcriptional code and disease map for adult retinal cell types. *Nat. Neurosci.* **15,** 487–495 (2012).
24. Strunnikova, N. V. *et al.* Transcriptome analysis and molecular signature of human retinal pigment epithelium. *Hum. Mol. Genet.* **19,** 2468–2486 (2010).
25. Xia, N. *et al.* Transcriptional comparison of human induced and primary midbrain dopaminergic neurons. *Sci. Rep.* **6,** 20270 (2016).
26. Zhang, Y. *et al.* An RNA-sequencing transcriptome and splicing database of glia, neurons, and vascular cells of the cerebral cortex. *J. Neurosci.* **34,** 11929–11947 (2014).
27. Zhang, Y. *et al.* Purification and Characterization of progenitor and mature human astrocytes reveals transcriptional and functional differences with mouse. *Neuron* **89,** 37–53 (2016).
28. Furukawa, T., Morrow, E. M. & Cepko, C. L. *Crx*, a novel *otx*-like homeobox gene, shows photoreceptor-specific expression and regulates photoreceptor differentiation. *Cell* **91,** 531–541 (1997).
29. Korf, H. W., White, B. H., Schaad, N. C. & Klein, D. C. Recoverin in pineal organs and retinae of various vertebrate species including man. *Brain Res.* **595,** 57–66 (1992).
30. Dennis, G. Jr *et al.* DAVID: database for annotation, visualization, and integrated discovery. *Genome Biol.* **4,** 3 (2003).
31. Huttenlocher, P. R. & Dabholkar, A. S. Regional differences in synaptogenesis in human cerebral cortex. *J. Comp. Neurol.* **387,** 167–178 (1997).
32. Scholvin, J. *et al.* Close-packed silicon microelectrodes for scalable spatially oversampled neural recording. *IEEE Trans. Biomed. Eng.* **63,** 120–130 (2016).
33. Fujisawa, S., Amarasingham, A., Harrison, M. T. & Buzsáki, G. Behavior-dependent short-term assembly dynamics in the medial prefrontal cortex. *Nat. Neurosci.* **11,** 823–833 (2008).
34. Stark, E. & Abeles, M. Unbiased estimation of precise temporal correlations between spike trains. *J. Neurosci. Methods* **179,** 90–100 (2009).
35. Zeman, S. & Lodge, D. Pharmacological characterization of non-NMDA subtypes of glutamate receptor in the neonatal rat hemisected spinal cord *in vitro*. *Br. J. Pharmacol.* **106,** 367–372 (1992).
36. Zhong, X. *et al.* Generation of three-dimensional retinal tissue with functional photoreceptors from human iPSCs. *Nat. Commun.* **5,** 4047 (2014).

Supplementary Information is available in the online version of the paper.

Acknowledgements We thank J.R. Brown, S. Hyman, G. Feng, Z. Fu, A. Schinder, L. Rubin, F. Rapino, former and present members of the Arlotta laboratory for insightful discussions and editing of the manuscript, A. Pollen and A. Kriegstein for sharing of human single-cell datasets and C. Cepko for sharing of antibodies, Y. Zhang for outstanding technical support, E. Zuccaro, F. Yates and S. Pavoni for helpful advice on culturing organoids. This work was supported by grants from the Stanley Center for Psychiatric Research, the Broad Institute of Harvard and MIT, and the Star Family Award of Harvard University to P.A. E.S.B. acknowledges NIH Director's Pioneer Award 1DP1NS087724. J.W.L. acknowledges support by IARPA, Conte and MURI Army Research Office. P.A. and E.S.B. are New York Stem Cell Foundation-Robertson Investigators.

Author Contributions P.A. and G.Q. conceived the experiments. G.Q. developed the long-term cultures of organoids and performed all immunohistochemical characterization with help from N.M. E.Z.M., G.Q., T.N. and M.G. performed all single-cell sequencing experiments. E.Z.M., G.Q., T.N., P.A. and S.A.M. analysed and interpreted the Drop-seq data. J.L.S., S.M.Y. and Z.M.W. performed electrophysiological experiments. J.S., J.P.K. and E.S.B. developed multi-electrode probes and helped J.L.S. adapt them to organoids. D.R.B. and J.W.L. performed electron microscopy work. P.A., G.Q., E.Z.M. and S.A.M. wrote the manuscript with contributions from all authors.

Author Information Reprints and permissions information is available at www.nature.com/reprints. The authors declare no competing financial interests. Readers are welcome to comment on the online version of the paper. Publisher's note: Springer Nature remains neutral with regard to jurisdictional claims in published maps and institutional affiliations. Correspondence and requests for materials should be addressed to P.A. (paola_arlotta@harvard.edu) and G.Q. (giorgia_quadrato@harvard.edu).

Reviewer Information *Nature* thanks F. Guillemot, S. Linnarsson and the other anonymous reviewer(s) for their contribution to the peer review of this work.

METHODS

Data reporting. No statistical methods were used to predetermine sample size. The investigators were blinded to organoid identity and age during experiments and outcome assessment.

Pluripotent stem cell culture. Human pluripotent stem cells used in these experiments were from the human 11a cell line[37] (gift from the Eggan laboratory, Harvard University), which we confirmed to be karyotypically normal. Cells were maintained in 10-cm tissue culture dishes (Corning) coated with 1% Geltrex membrane matrix (Thermo Fisher Scientific) in mTeSR medium (StemCell Technologies). Pluripotent stem cells and colonies were dissociated with the Gentle Cell Dissociation Reagent (StemCell Technologies). All human pluripotent stem cells were maintained below passage 50 and confirmed negative for mycoplasma.

Long-term cultures of human brain organoids. Cerebral organoids were generated using a modified version of a previously published protocol[10]. Embryoid bodies were derived by dissociating pluripotent stem cell colonies and plating 2,500 single cells in each well of a 96-well plate. Embryoid bodies were cultured as previously described[10]. After five days in culture, embryoid bodies were transferred to intermediate induction medium (IIM), consisting of DMEM/F12, 6% KOSR (Thermo Fisher Scientific), 0.9% FBS (GIBCO), 0.7% N2 supplement (Invitrogen), Glutamax (Invitrogen), minimum-essential-media non-essential amino acids (MEM-NEAA) (Thermo Fisher Scientific), heparin 0.7 μg ml^{-1} (Sigma). Two days after plating in IIM, 500 μl of neural induction medium (NIM) was added to each well. Following neural induction, organoids were embedded in Matrigel and transferred to cerebral differentiation medium (CDM) as described previously[10]. A total of 40 organoids were added to each spinner flask, and medium was changed once every six days for the duration of the culture process. After one month, BDNF was added to the CDM medium at a concentration of 14 ng ml^{-1}. Cerebral organoids were cultured for up to 13 months. A step-by step protocol describing the long-term culture of human brain organoid can be found at Protocol Exchange[39].

For induction of hypoxia, six-month organoids were cultured in cerebral differentiation medium supplemented with 100 μM cobalt (II) chloride (Millipore) in a conventional incubator (37 °C; 5% CO_2) for 24 h before fixation.

Histology and immunofluorescence. Cerebral organoids were fixed by immersion in 4% paraformaldehyde (Electron Microscopy Services), cryoprotected in 30% sucrose solution and then embedded in optimum cutting temperature (OCT) compound (Tissue Tek). Organoids were then cryosectioned at a thickness of 14 or 30 μm.

Immunohistochemistry was performed as previously described[38]. Primary antibodies and dilutions used were as specified in Supplementary Table 1. Fluorescently conjugated secondary antibodies used were goat anti-rabbit IgG Alexa Fluor 488, 546, 647 (Life Technologies A11070, A11071, A21246), goat anti-chicken IgG Alexa Fluor 488, 546, 647 (Life Technologies A11039, A11040, A21449), goat anti-rat 488, 546, 647 (Life Technologies A11006, A11081, A21247), goat anti-mouse IgG Alexa Fluor 488, 546, 647 (Life Technologies A11017, A11018, A21237), Alexa Fluor donkey anti-mouse 488 (Life Technologies A21202), Alexa Fluor donkey anti-rabbit 488 (Life Technologies A10036), Alexa Fluor donkey anti-rat 488 (Life Technologies A21208), Alexa Fluor donkey anti-mouse 546 (Life Technologies A10036), Alexa Fluor donkey anti-goat 546 (Life Technologies A11056), Alexa Fluor donkey anti-mouse (Life Technologies A31571) and Alexa Fluor donkey anti-rabbit 647 (Life Technologies A10040). Secondary antibodies were diluted 1:1,200. Rhodopsin immunohistochemistry was performed without Triton X-100 or Tween 20 to preserve membrane integrity and the signal was amplified using biotin (1:500, Vector BA9200) and streptavidin (1:600, Thermo Fisher S32354) conjugates. Cell nuclei were stained with Hoechst (1:5,000; Invitrogen), and slides were mounted using Fluoromount-G mounting medium.

Microscopy and image analysis. All mounted sections were imaged using a Nikon Eclipse Ti microscope, analysed with NIS Elements analysis software and processed using ImageJ. Confocal images were obtained using a Zeiss 700 confocal microscope. Images were collected and analysed using the Zen 2010 program. For electron microscopy, images were processed using ImageJ, manually segmented using VAST Lite (freely available at https://software.rc.fas.harvard.edu/lichtman/vast/), and rendered in 3ds Max (Autodesk, Inc.).

Drop-seq single-cell RNA sequencing. For the 6 months dataset, we sequenced 19 organoids from 4 bioreactors: 4 organoids from bioreactor 1 (Org1A, 3,547 cells; Org1B, 3,463 cells; Org1C, 3,698 cells; Org1D, 2,811 cells), 3 organoids from bioreactor 2 (Org2A, 2,238 cells; Org2B, 3,159 cells; Org2C, 2,708 cells), 4 organoids from bioreactor 3 (Org3A, 4,225 cells; Org3B, 2,557 cells; Org3C, 3,614 cells; Org3D, 11,061 cells) and 8 organoids from bioreactor 4 (Org4A, 1,656 cells; Org4B, 1,663 cells; Org4C, 1,795 cells; Org4D, 2,151 cells; Org4E, 3,407 cells; Org4F, 7,443 cells; Org4G, 2,905 cells; Org4H, 2,788 cells). For the 3 months dataset, we sequenced 12 organoids from bioreactor 6 (8,478 cells) and bioreactor 7 (6,924 cells).

A step-by-step protocol describing human brain organoid single-cell dissociation can be found on Protocol Exchange[39]. Droplets containing single cells and barcoded microparticles were generated and processed as previously described[11]. In brief, droplets were collected and beads were recovered and processed for immediate reverse transcription. The resulting cDNA was amplified, fragmented and further amplified using the Nextera XT DNA library preparation kit. Sequencing was performed on the Illumina NextSeq 500.

Clustering of cells derived from six-month-old organoids was performed using the Seurat R package[12], with some modifications from the procedure described previously[11]. Clustering was done in two iterative rounds of principal component analysis. First, digital gene expression matrices were column-normalized and log-transformed. Cells with fewer than 400 expressed genes were removed from analysis. A set of variable genes was then identified by binning the average expression of all genes into 300 evenly sized groups and computing the median dispersion (variance divided by the mean) in each bin. Genes were selected for inclusion in principal component analysis that had higher than twice the median dispersion, minus the minimum value (final set: 1,568 genes). The edges of a nearest neighbour graph were generated by computing the fraction of shared nearest neighbours among cells in the first 20 principal component dimensions using the approximate nearest neighbours package (ANN) in R (CRAN), setting the *k* parameter to 25 (BuildSNN function in Seurat). A first round of clustering with the Louvain modularity-based community detection algorithm[40] set at a resolution of 0.01 was used to generate a total of 10 first-round clusters (FindClusters function in Seurat). The largest 50% of the cells from each of these clusters was again subjected to gene selection and principal components analysis. These principal components were evaluated for statistically significant gene expression signals using the Jackstraw method[11,41] (JackStraw function in Seurat). At most, 15 principal components were used in this second round of clustering by Louvain, with the resolution parameter set at 3. The resulting clusters were compared pairwise for differential expression, as previously described[11], and clusters with fewer than 10 genes that were differentially expressed by more than twofold were merged, producing 202 clusters. For analysis of organoid-to-organoid variability, organoids were excluded from a given cluster if they contributed less than 1% of the cells in that cluster.

Correlation analysis between gene expression in a dataset of human fetal cortex[22] against the astrocyte cluster (c2) and the identified subclusters of the forebrain cluster (c4) was performed using the log average expression of a set of 104 genes, identified by taking the top 10 most differentially expressed genes for each cluster pair in the published fetal cortex dataset (some of which overlapped) as the most informative for distinguishing the reported endogenous cell classes of the cortex. We then constructed expression profiles for the six organoid cell groups and measured the correlation of gene expression levels for the 104 endogenous genes, comparing each of the endogenous cortical cell classes to each of the organoid cell groups. For the retinal subclusters (subclusters of c5), we repeated this correlation analysis against a dataset of the postnatal day 14 mouse retina[11], using 110 genes, identified by taking the top 10 most enriched genes from the 11 major cell classes (horizontal cells, retinal ganglion cells, amacrine cells, photoreceptors, bipolar cells and six glial retinal types) in the mouse dataset and correlating against the expression profiles of the orthologous human genes in the six organoid retinal cell groups.

Electron microscopy. An eight-month-old organoid was immersion-fixed in 2.5% paraformaldehyde, 2.5% glutaraldehyde in 0.1 M sodium cacodylate buffer (EMS, 15949) at room temperature for 24 h. The organoid was washed in cold 0.15 M sodium cacodylate buffer (Caco buffer), embedded in 4% low-melt agarose and sectioned into 100-μm thick slices (Leica Vibratome) in cold Caco buffer (Extended Data Fig. 6). Three slices were selected for further processing. The results shown in Fig. 3 and Extended Data Fig. 6 come from one of those slices.

Preparation for electron microscopy was similar to previously described methods[41]. In brief, sections were washed in cold Caco buffer and stained for 2 h in reduced 2% osmium tetroxide solution (with 15 mg ml^{-1} potassium ferrocyanide) on ice, washed, incubated in 1% thiocarbohydrazide solution for 30 min, washed again and finally stained with 2% osmium tetroxide solution for 1 h (ROTO method). Slices were then dehydrated in a series of ascending ethanol concentrations, followed by acetone and propylene oxide, infiltrated with mixtures of epoxy resin (variants of EPON) and propylene oxide and embedded in 100% epoxy resin and cured at 60 °C for two weeks. Blocks were trimmed and sectioned at 40 nm slice thickness with a Leica EM UC6 Ultramicrotome and serial sections were collected on carbon-coated Kapton tape using an ATUM[42]. Strips of tape were mounted on silicon wafers and sections were post-stained with 2% uranyl acetate and lead citrate (Leica Ultrastain). Slices were then imaged in a Zeiss Sigma scanning electron microscope.

A stack of 136 slice images was acquired using backscatter electron imaging (9 kV, 3 μs dwell time per pixel, $12{,}288^2$ pixels at 4 nm resolution). A roughly

aligned region of $4{,}096^2$ pixels was cropped from the images and aligned using ImageJ (Linear Stack Alignment with SIFT, using expected transformation: Affine). The resulting aligned image stack was imported into VAST Lite for manual segmentation. 3D rendering was done in in 3ds Max (Autodesk, Inc.). Data analysis was performed in Matlab (The Mathworks, Inc.). We noted that axons, more than dendrites, appeared to preferentially run parallel to the organoid surface (Wilcoxon rank-sum test, $P < 10^{-5}$; Fig. 3i and Supplementary Video 2). For the Wilcoxon rank-sum test we first performed a principal component analysis of the point cloud of each axon and dendrite, and used the vertical components of each largest principal component of all axons versus all dendrites.

Electrophysiology. Cerebral organoids were randomly selected and transferred from the culture flask to a recording chamber containing artificial cerebrospinal fluid composed of (in mM) NaCl (125.0), D-Glucose (10.0), $NaHCO_3$ (26.2), KCl (3.5), NaH_2PO_4 (1.3), $MgCl_2$ (1.0), $CaCl_2$ (1.2), L-Ascorbic acid (1.0) and Na-Pyruvate (1.0), bubbled with carbogen (95% O_2, 5% CO_2). In the recording chamber, the organoid was immobilized by placing it on a small grid of spikes. Prior to recording, the organoids were initially held at 32 °C for 30 min, followed by a further 30 min acclimatisation at 36 °C (the recording temperature). The temperature of the recording chamber was monitored and maintained by a temperature control unit (TC-344C, Warner Instruments), and a custom built heating platform. During acclimatization and electrophysiological recordings, the organoids were maintained in the absence of ambient light. Extracellular silicon probes were positioned by a micromanipulator (Scientifica PatchStar) under infrared illumination (850 nm LED) using a digital microscope (Dino-Lite Edge AM4115-FIT). Extracellular neurophysiological signals were recorded using high-density silicon probes[32] with a two-column, 32-row configuration of $9 \times 9\,\mu m$ poly(3,4-ethylenedioxythiophene) (PEDOT)-electroplated gold recording sites of $12\,\mu m$ pitch (Extended Data Fig. 7a, top). Each recording site is connected to the outside by insulated nanofabricated wires, running along the length of the probe shank (visible in Extended Data Fig. 7a as grey lines flanking the recording sites). The shank width is tapered from 35 to $60\,\mu m$ wide, and is $15\,\mu m$ thick. Signals were processed and digitized on a headstage proximal to the silicon probe (Intan RHD2000 chip, $30\,kS\,s^{-1}$ per channel, 0.1 Hz high pass filter, 7.6 kHz anti-aliasing filter, 16-bit ADC), then acquired by a NeuroNexus SmartBox system. Wide-band data were stored for analysis. Spike detection was carried out by SpikeDetekt. The initial spike clustering was done by an unsupervised masked expectation-maximization algorithm (KlustaKwik), followed by a stage of manual curation aided by KlustaViewa software (full procedure is described in ref. 43). In order to show raw signal (Fig. 4b), we applied a 117-Hz high-pass Daubechies 4 wavelet filter.

Spontaneous neuronal activity was recorded for at least 10 min. A cerebral organoid was classified as not active when no spontaneous action potentials were detected during 40 min of recording in at least 3 different recording sites. The 99% confidence bounds for the Fano factor were approximated by a gamma distribution[44]. Mono-synaptic connections were identified by the detection of peaks or troughs with a short time lag (<5 ms) in the spike-train cross-correlograms[33,34]. The statistical threshold for the identification of connected pairs was set at the 99.9th percentile of the cumulative Poisson distribution for the estimated spike rate, which was calculated by convolving the cross-correlogram (0.5 ms bins) with a Gaussian window (s.d., 10 ms).

Light stimulation was controlled by in-house Matlab scripts. In brief, a National Instruments board (NI PCIe-6323, X Series DAQ) was used to deliver TTL pulses to an external LED driver (LEDD1B, ThorLabs). For light stimulation, a 530 nm LED (Thorlabs, M530L3) was single band-pass filtered (11 nm bandwidth, Semrock FF01-530/11) and collimated. Using a calibrated meter and photodiode (PM100D and S130C, Thorlabs), the maximum LED power output was set to $300\,\mu W\,cm^{-2}$, and the final output controlled by pulse-width modulation. During light stimulation, ninety 200-ms pulses of 530 nm light were delivered at 0.2 Hz (the first 30 were $30\,\mu W\,cm^{-2}$, the second 30 were at $100\,\mu W\,cm^{-2}$, the final 30 were at $300\,\mu W\,cm^{-2}$).

For the analysis of the light experiment, the mean spike rate recorded during a 5-min period post-light stimulus was normalized to a 5-min period immediately before light stimulation. The baseline normalized spike rate was then fit by a series of Gaussian mixture models, with 1–4 components. Minimization of the Bayes information criterion was used to identify the optimal number of components. Post-fitting, data was partitioned according to the fit component with the largest posterior probability, weighted by the component probability. All analysis was done in Matlab, using Statistics Toolbox version 9.0 (fitgmdist.m and cluster.m). Four units were excluded from analysis based on a mean baseline spike rate <0.1 Hz (two 11a cell units and two HUES66 units).

Stock solutions of 2,3-dioxo-6-nitro-1,2,3,4-tetrahydrobenzo[*f*]quinoxaline-7-sulfonamide disodium salt (NBQX disodium salt, Abcam; 100 mM) and tetrodotoxin citrate (TTX, Abcam; 10 mM) were prepared in ddH_2O.

All descriptive statistics and statistical tests were performed in Matlab (version 8.3, R2014a, The MathWorks, Inc.), using the Statistics Toolbox (version 9.0, R2014a, The MathWorks, Inc.). The Lilliefors test was used to test for normality of data distributions. As the null hypothesis that the mean spike rates are normally distributed was rejected at the 5% level ($P < 0.001$), appropriate non-parametric tests for paired and independent datasets were used to test for significance. All datasets met the assumptions of the applied statistical tests. Mean spike rate data are presented as Tukey style box plots, showing the 1st, 2nd and 3rd quantile (Q1, median and Q3, respectively; inter-quartile range, IQR = Q3 − Q1). Box plot whiskers extend to the most extreme data points between Q1 − 1.5IQR and Q3 + 1.5IQR. For illustrative purposes, all data points outside the whiskers are plotted individually. When comparing groups, the equality of the variance was tested at the 5% significance level by a two-tailed squared-ranks test. All statistical tests applied to the electrophysiological data were two-tailed, with a 5% significance level. A step-by-step protocol describing eletrophysiological characterization of human brain organoid can be found at Protocol Exchange[39].

Data availability. Single-cell RNA sequencing data that support the findings of this study have been deposited at NCBI GEO, accession number GSE86153. The secondary single-cell RNA sequence datasets used for reanalysis are the mouse retinal dataset available at GEO with accession number GSE63473 and the human fetal brain and organoid dataset, available at the Database of Genomic Structural Variation (dbGaP), study accession number dbGaP: phs000989.v2.p1.

37. Boulting, G. L. *et al.* A functionally characterized test set of human induced pluripotent stem cells. *Nat. Biotechnol.* **29,** 279–286 (2011).
38. Quadrato, G. *et al.* Nuclear factor of activated T cells (NFATc4) is required for BDNF-dependent survival of adult-born neurons and spatial memory formation in the hippocampus. *Proc. Natl Acad. Sci. USA* **109,** E1499–E1508 (2012).
39. Quadrato, G. *et al.* Long-term culture and electrophysiological characterization of human brain organoids. *Protoc. Exch.* http://dx.doi.org/10.1038/protex.2017.049 (2017).
40. Waltman, L. & van Eck, N. J. A smart local moving algorithm for large-scale modularity-based community detection. *Eur. Phys. J. B* **86,** 471 (2013).
41. Chung, N. C. & Storey, J. D. Statistical significance of variables driving systematic variation in high-dimensional data. *Bioinformatics* **31,** 545–554 (2015).
42. Kasthuri, N. *et al.* Saturated reconstruction of a volume of neocortex. *Cell* **162,** 648–661 (2015).
43. Rossant, C. *et al.* Spike sorting for large, dense electrode arrays. *Nat. Neurosci.* **19,** 634–641 (2016).
44. Eden, U. T. & Kramer, M. A. Drawing inferences from Fano factor calculations. *J. Neurosci. Methods* **190,** 149–152 (2010).

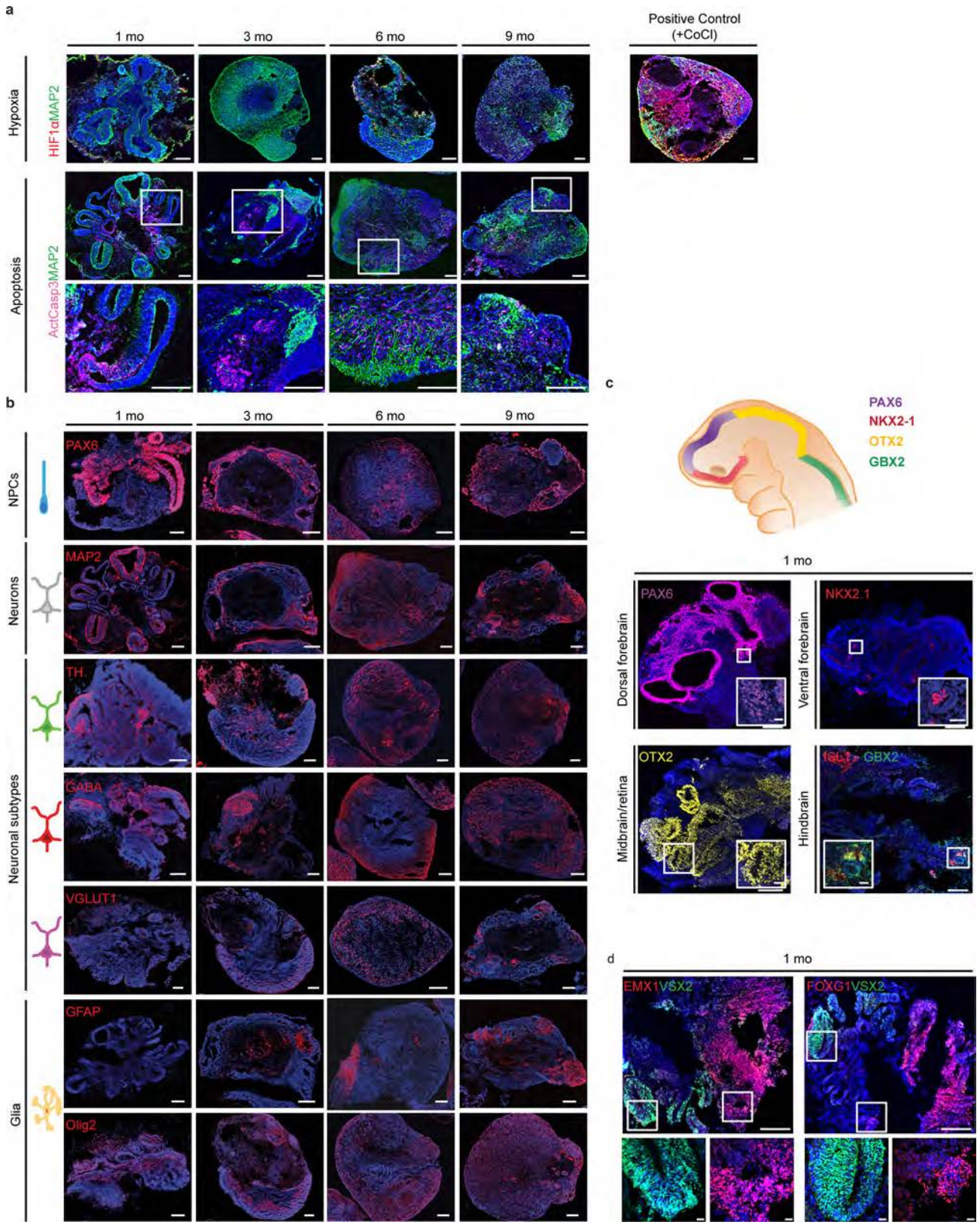

Extended Data Figure 1 | Time-course of expression of selected marker genes in human brain organoids. a, Top, expression of the hypoxia marker HIF1α over one to nine months of culture, and positive control (a six-month-old organoid treated with cobalt (II) chloride (CoCl), an activator of the hypoxia signalling pathway). Bottom, expression of the apoptosis marker, active caspase 3 (ActCasp3) and the neuronal marker (MAP2), over one to nine months of culture. **b**, Expression of markers for progenitor, neuronal and glial populations over one to nine months of culture. **c**, One-month-old brain organoids exhibit early brain regionalization, expressing markers of forebrain (PAX6 and NKX2.1), midbrain (OTX2) and hindbrain (GBX2) progenitors. **d**, One-month-old brain organoids express the cortical marker EMX1, the forebrain marker FOXG1 and the retina marker VSX2, with spatial segregation between regions positive for forebrain versus retinal markers. Scale bars, 250 μm and 20 μm (insets).

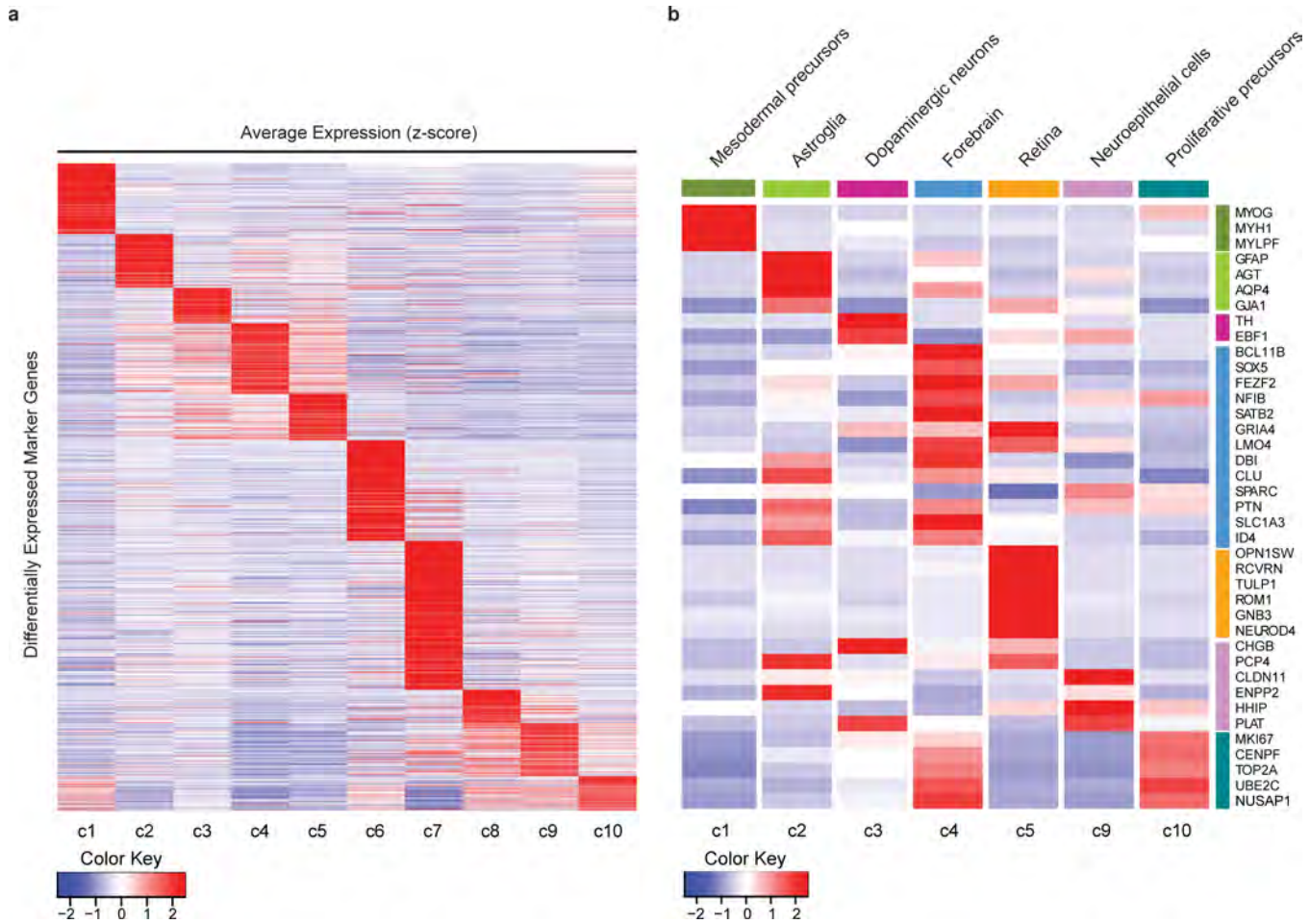

Extended Data Figure 2 | Decoding of the identity of cell types within the main clusters. a, Heatmap of differentially expressed cell-type marker genes across each of the 10 main clusters. For gene lists and *P* values, see Supplementary Table 2, for references of cluster identification, see Extended Data Table. 1. **b**, Heatmap of average expression for representative marker genes and cell-type classification of the main clusters from the six-month-old organoid dataset.

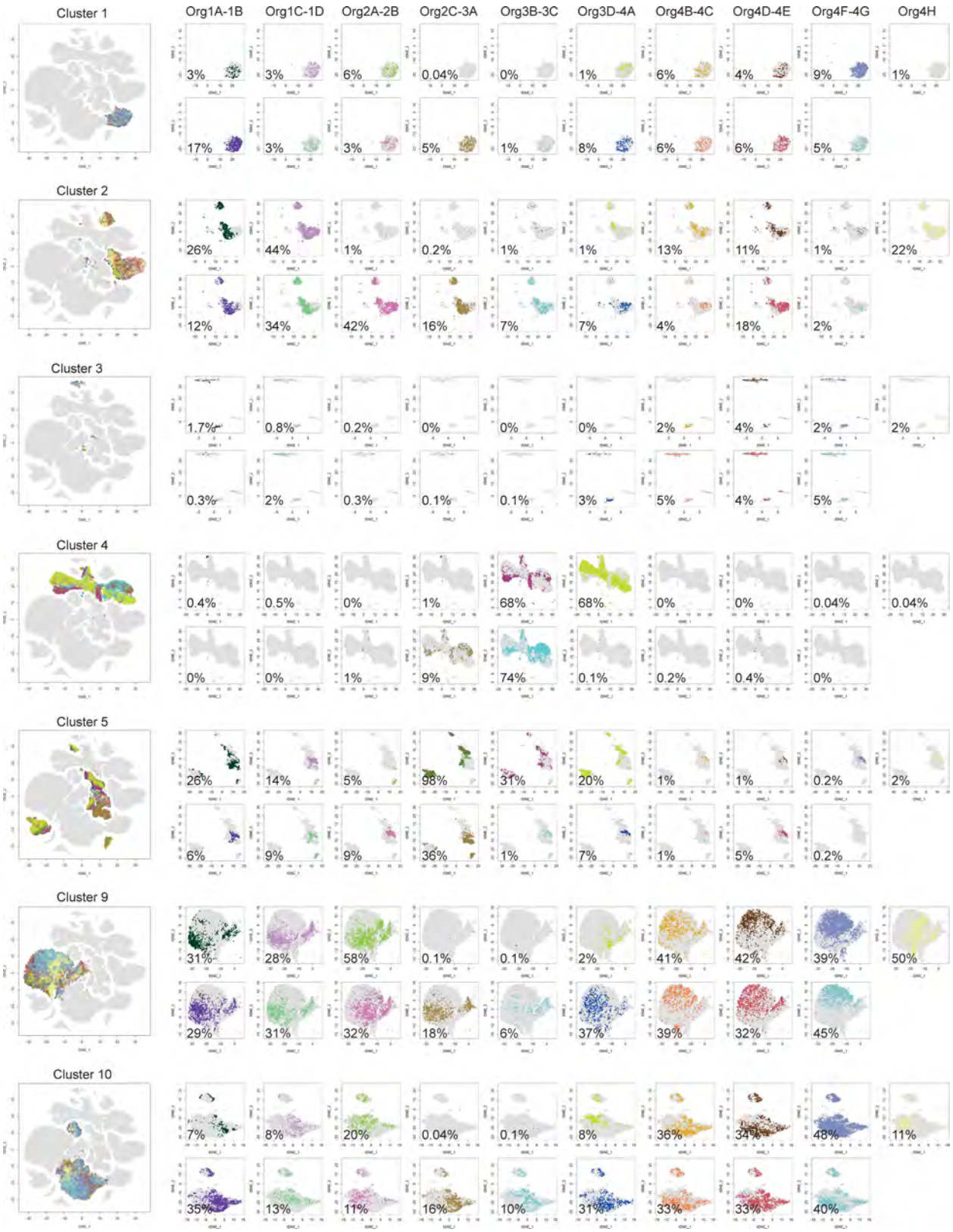

Extended Data Figure 3 | Quantifying variability among organoids. *t*SNE plots depicting the proportion of cells each organoid contributed to each cell-type cluster. The cells are colour-coded by the organoid of origin. The large plot shows the entire cluster, and the smaller plots show the contribution of each individual organoid, labelled with the percentage of cells within the cluster contributed by that organoid.

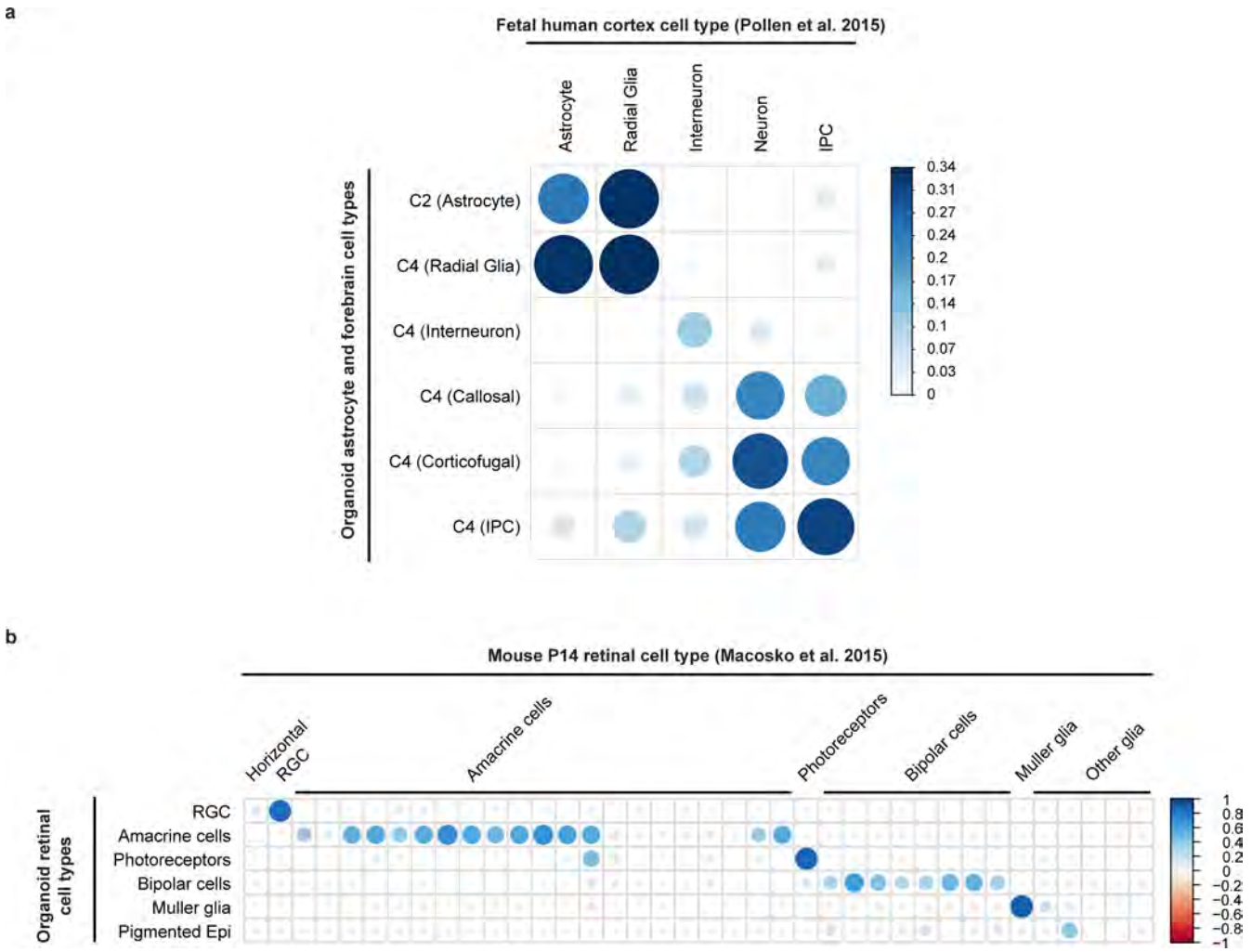

Extended Data Figure 4 | Correlation analysis for organoid cell types compared to the human fetal cortex and mouse retina. a, Correlation between expression patterns of highly variable genes between cell populations within a previously published single-cell RNA-seq dataset of the human fetal cortex[22] against the organoid astroglial cluster (c2) and the identified subclusters of the forebrain cluster (c4). IPC, intermediate progenitor cells. **b**, Correlation between expression patterns of highly variable genes between cell populations within a previously published single-cell RNA-seq dataset of postnatal day (P)14 mouse retina[11] and the cell populations identified within the retinal cluster (c5) in our organoid dataset. Pigmented Epi, pigmented epithelium; RGC, retinal ganglion cells. Colour keys (and dot sizes) represent the range of the coefficients of determination (r^2) in each analysis.

a

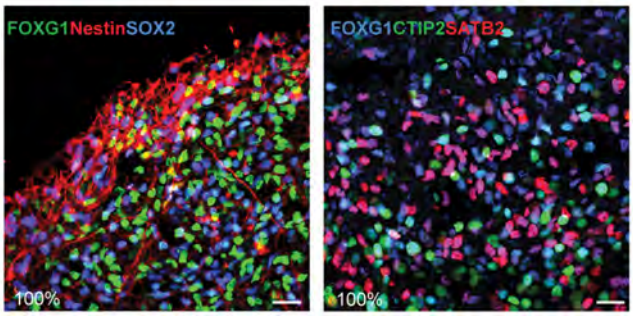

b

	IN	IPC	CfuPN	CPN	RG	Total Classified	%IN	%IPC	%CfuPN	%CPN	%RG
Org3A	4	9	18	45	43	119	3.361	7.563	15.126	37.815	36.134
Org3B	68	1	1	134	357	561	12.121	0.178	0.178	23.886	63.636
Org3C	7	157	563	110	281	1118	0.626	14.043	50.358	9.839	25.134
Org3D	6	8	5	1285	1327	2631	0.228	0.304	0.19	48.841	50.437

c

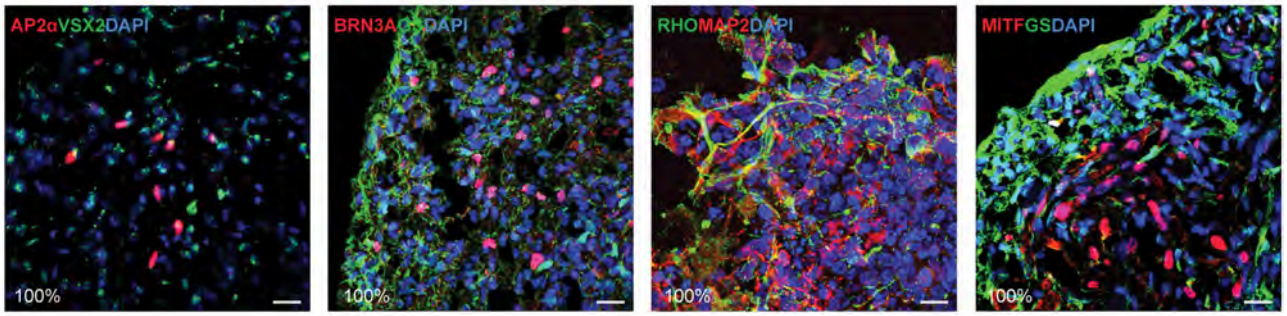

d

	MG	PE	PHOTO	RGC	BI	AM	Total Classified	%MG	%PE	%PHOTO	%RGC	%BP	%AC
Org1A	17	39	8	4	3	1	72	23.61	54.17	11.11	5.56	4.17	1.39
Org1B	0	1	3	0	0	0	4	0	25	75	0	0	0
Org1C	0	8	1	38	0	0	47	0	17.02	2.13	80.85	0	0
Org1D	0	62	4	1	2	1	70	0	88.57	5.71	1.43	2.86	1.43
Org2A	0	93	0	0	0	0	93	0	100	0	0	0	0
Org2B	0	1	0	3	0	133	137	0	0.73	0	2.19	0	97.08
Org2C	252	1	801	0	294	306	1654	15.24	0.06	48.43	0	17.78	18.5
Org3A	0	133	6	1	2	0	142	0	93.66	4.23	0.7	1.41	0
Org3B	27	0	95	0	18	46	186	14.52	0	51.08	0	9.68	24.73
Org3C	0	5	0	2	0	0	7	0	71.43	0	28.57	0	0
Org3D	31	36	257	0	5	7	336	9.23	10.71	76.49	0	1.49	2.08

Extended Data Figure 5 | Distribution and reproducibility of forebrain and retinal cell types across organoids. a, Immunohistochemical detection in a six-month-old organoid of the forebrain marker FOXG1 with the progenitor markers Nestin and SOX2 (left) and of FOXG1 with the corticofugal projection neuron marker CTIP2 and the callosal projection neuron marker SATB2 (right), all showing extensive colocalized coexpression, which was observed in all organoids examined (6 out of 6). **b**, Number of cells assigned to each cortical cell type in individual organoids from flask 3, and the percentage of each cell type out of all classified cortical cells in that organoid. **c**, Immunohistochemical detection of retinal cell types in six-month-old organoids shows expression of known markers for amacrine cells, bipolar cells, retinal ganglion cells, Müller glia, rods and retinal pigmented epithelium, observed across all organoids in every flask, $n = 11$; 3 bioreactors. **d**, Number of cells assigned to each retinal cell type in individual organoids from flasks 1–3, and the percentage of each cell type out of all classified retinal cells in that organoid. AC, amacrine cells; BP, bipolar cells; CfuPN, corticofugal projection neurons; CPN, callosal projection neurons; IN, interneurons; IPC, intermediate progenitor cells; MG, Müller glia; PE, pigmented epithelium; photo, photoreceptors; RG, radial glial cells; RGC, retinal ganglion cells.

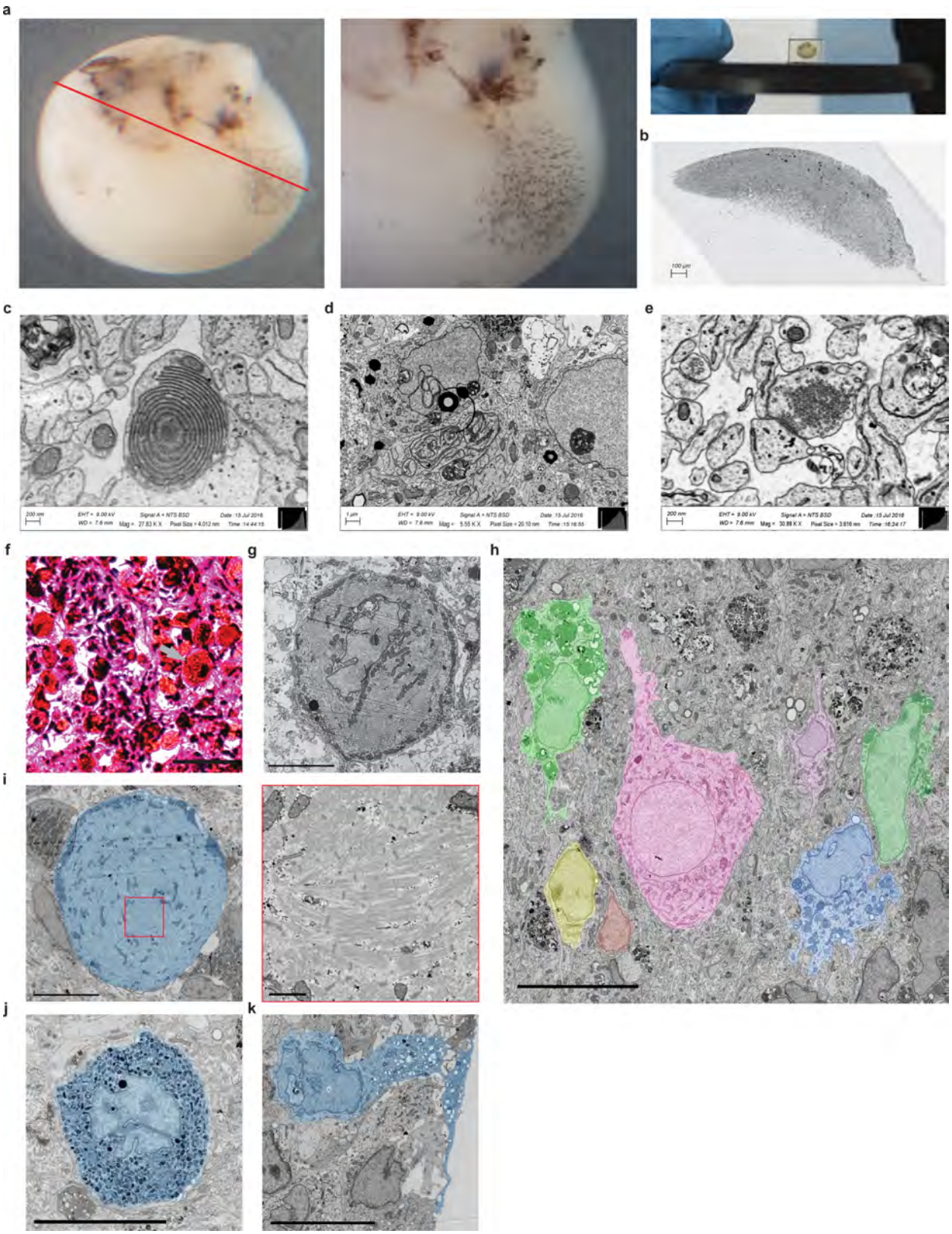

Extended Data Figure 6 | Electron microscopy of an eight-month-old human brain organoid. **a**, Whole organoid before vibratome sectioning shows regional structures. The red line shows the approximate location of the vibratome slice. **b**, Example 40-nm section. **c**. Regular finger-like membrane stack could indicate development of the outer segment of a retinal rod cell. **d**, Stacked endoplasmic reticulum. **e**, Example synapse with crystalline-looking arrangement of vesicles. **f**, Putative muscle cell characterized by a large cell body with a diameter of about 30 μm highlighted in an organoid section stained with eosin and haematoxylin. **g**, Example of a muscle cell showing a distribution of the mitochondria near the cell surface, which is typical for muscle cells. **h**, Several cell bodies with different morphologies and cytoplasm content highlighted in colour. **i**, Large cell body with muscle fibres highlighted in blue. Inset (red square) shows muscle fibres with sarcomeres. **j**, One of the dark cell bodies appearing as dark spots on the organoid surface. **k**, Cell reaching to the surface of the organoid. Scale bars, 50 μm (**f**), 10 μm (**g**–**k**) and 1 μm (**i**, inset).

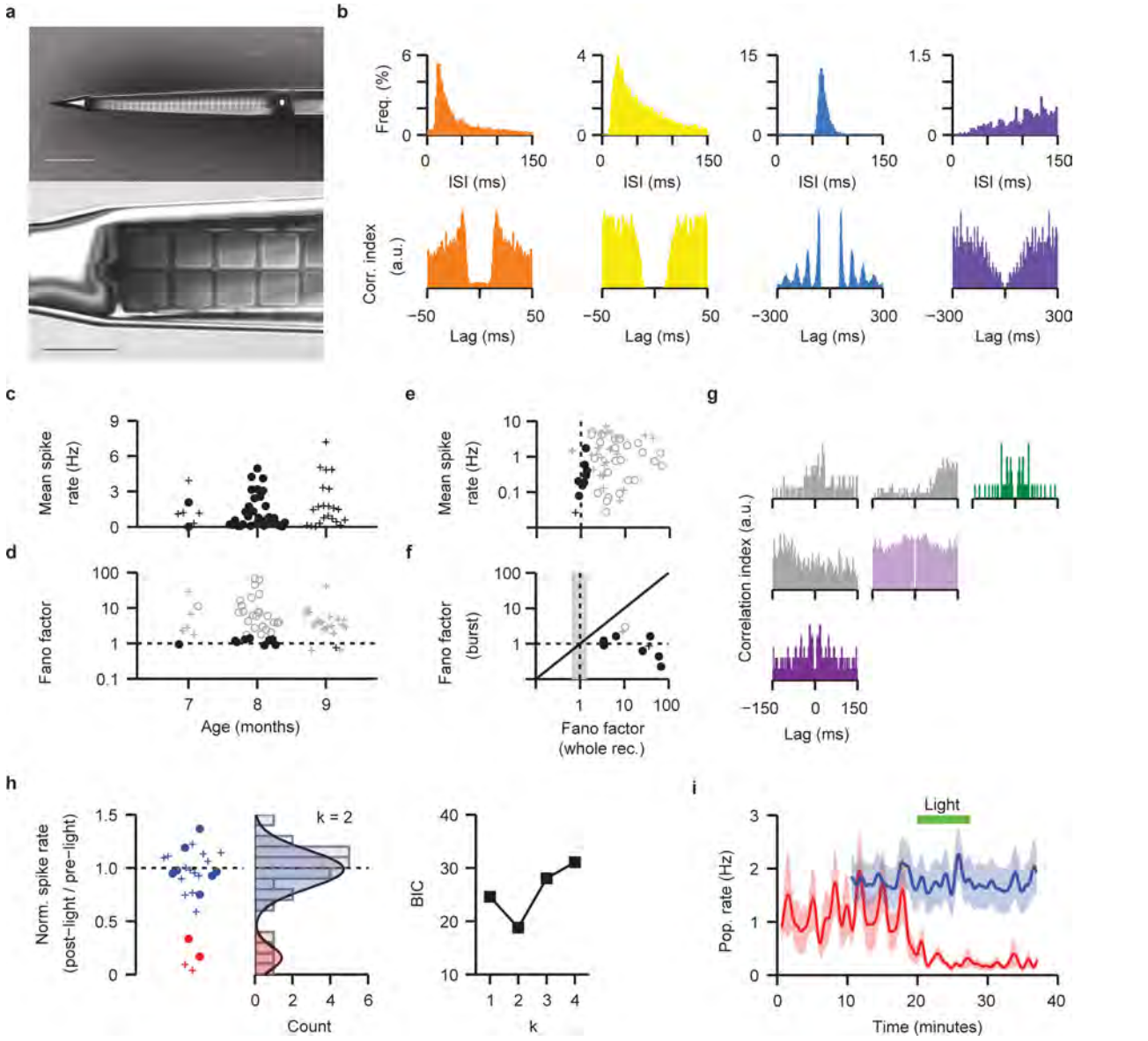

Extended Data Figure 7 | Statistical structure of spontaneous activity. **a**, Electron micrographs of a 64-channel probe shank tip (Fig. 4a). Scale bars, 100 μm (top) and 20 μm (bottom). **b**, Example inter-spike interval (ISI, top) and auto-correlogram (bottom) plots for spontaneous activity recorded from 4 prototypical units; a.u., arbitrary units; freq., frequency. **c**, Plot of the mean spike rate in 11a cells (dots) and HuES66 (+) organoids recorded at 7–9 months. The difference between the median of the mean spike rates is not significant across lines (11a cells, $n = 34$ cells, 12 recording sites, 7 organoids, median = 0.662 Hz, Q1–Q3 = 0.186–2.071 Hz; HuES66 $n = 27$ cells, 9 recording sites, 8 organoids, median = 1.186 Hz, Q1–Q3= 0.463–2.848 Hz; two-tailed Wilcoxon rank-sum test, $z = -1.47$, $P = 0.14$; furthermore, the variance is not significantly different, squared-ranks test, $z = -1.47$, $P = 0.141$). **d**, Plot of the Fano factor against organoid age. **e**, Plot of mean spike rate against the Fano factor ($n = 61$ neuronal units, from 15 organoids). Fano factors outside the expected 99% confidence bounds for a Poisson distribution are plotted in grey (otherwise black). **f**, Plot of the Fano factors calculated across the whole recording versus the first second of population bursts. Shading, 99% confidence bounds for a whole-recording Fano factor of 1. Black symbols, Fano factor close to 1, consistent with a stationary Poisson-distributed system. **g**, Spike train auto-correlogram (colour-coded as in Fig. 4g) and cross-correlogram (grey) for the three units presented in Fig. 4g. **h**, Left, baseline normalized spike rate ($n = 25$ cells, 10 organoids; 11a cells, $n = 9$ cells, 4 organoids; HuES66, $n = 16$ cells, 6 organoids); the clustering of data of responders (red) and non-responders (blue). Middle, count histogram of the left data plot overlaid by the optimal Gaussian mixture model (number of components $k = 2$, see methods; $\mu_k = k$th mean, $\sigma_k = k$th s.d.). The underlying distributions are shaded ($\mu_1 = 0.16$, $\sigma_1 = 0.11$, mixing proportion = 0.16; $\mu_2 = 0.99$, $\sigma_2 = 0.18$, mixing proportion = 0.84). Right, plot of the Bayes information criterion (BIC) generated for the Gaussian mixture models with k components. **i**, Population averaged activity for light responsive (red, $n = 4$), and non-responsive (blue, $n = 21$), neurons; error envelope (shaded) is the s.e.m. In the four responsive organoids, light stimulation attenuated firing rate in 4 out of 5 isolated neurons.

Extended Data Table 1 | References used for cluster identification in Extended Data Fig. 2

Cell type	References
Astroglia (c2)	Zhang et al. 2016 [27], Cahoy et al. 2008 [16], Marques et al. 2016 [20]
Dopaminergic Neurons (c3)	Xia et al. 2016 [25]
Intermediate Progenitor Cells (c4)	Pollen et al. 2015 [22]
Corticofugal Neurons (c4)	Arlotta et al. 2005 [15], Molyneaux et al. 2009 [21], Lake et al. 2016 [19]
Callosal Projection Neurons (c4)	Arlotta et al. 2005 [15], Molyneaux et al. 2009 [21], Lake et al. 2016 [19]
Cortical Interneurons (c4)	Pollen et al. 2015 [22]
Radial Glia (c4)	Pollen et al. 2015 [22], Camp et al. 2015 [17]
Retinal Ganglion Cells (c5)	Macosko et al. 2015 [11], Siegert et al. 2012 [23]
Amacrine Cells (c5)	Macosko et al. 2015 [11], Siegert et al. 2012 [23]
Photoreceptors (c5)	Macosko et al. 2015 [11], Siegert et al. 2012 [23]
Bipolar Cells (c5)	Macosko et al. 2015 [11], Siegert et al. 2012 [23]
Pigmented Epithelium (c5)	Strunnikova et al. 2010 [24]
Muller Glia (c5)	Macosko et al. 2015 [11]
Proliferative Precursor Cells (c10)	Camp et al. 2015 [17], Cahoy et al. 2008 [16], Darmanis et al. 2015 [18]